geosciences

MDPI

Article

Methane Derived Authigenic Carbonate (MDAC) Aragonite Cemented Quaternary Hardground from a Methane Cold Seep, Rathlin Basin, Northern Ireland: $\delta^{13}C$ and $\delta^{18}O$ Isotopes, Environment, Porosity and Permeability

Jim Buckman [1,*], Terry Donnelly [2], Zeyun Jiang [1], Helen Lewis [1] and Alastair Ruffell [3]

1 Institute of GeoEnergy Engineering, School of Energy Geoscience Infrastructure and Society, Heriot-Watt University, Riccarton, Edinburgh, Scotland EH14 4AS, UK; zeyun.jiang@hw.ac.uk (Z.J.); H.lewis@hw.ac.uk (H.L.)

2 Stable Isotope Laboratory, Scottish Universities Environmental Research Centre, East Kilbride, Scotland G75 0QF, UK; terry.donnelly@glasgow.ac.uk

3 Archaeology, Geography and Palaeoecology, School of Natural and Built Environment, Queen's University Belfast, Elmwood Avenue, Belfast, Northern Ireland BT7 1NN, UK; a.ruffell@qub.ac.uk

* Correspondence: j.buckman@hw.ac.uk

Received: 14 May 2020; Accepted: 29 June 2020; Published: 3 July 2020

Abstract: A block of sandstone retrieved by divers from near Rathlin Island, Co. Antrim, Northern Ireland, represents an aragonite cemented sand formed during the Quaternary. Strongly negative $\delta^{13}C$ of the aragonite cement (−50 to −60‰ $\delta^{13}C$) indicates that the hardground was formed by the anaerobic oxidation of methane (AOM), resulting in the formation of a methane-derived authigenic carbonate (MDAC) hardground. Such hardgrounds have previously been recorded as forming extensive pavements in deeper waters in the mid Irish Sea (e.g., Croker Carbonate Slabs), although the latter also contains high-magnesium calcite. Sand was initially deposited as part of a storm lag deposit, with a reworked bivalve and gastropod fauna. This sand was then colonised by a probable crustacean fauna, producing horizontal open dwelling burrows (*Thalassinoides*). After aragonite cementation, the hardground was colonised by boring bivalves, with slightly negatively elevated levels of $\delta^{13}C$. Finally, the hardground was colonised by an encrusting fauna (bryozoans, calcareous algae and serpulids), by then in warmer seas. Continued depleted levels of $\delta^{13}C$ present within the encrusting fauna (−1 to −5‰ $\delta^{13}C$) indicate continued methane generation and seepage, which may still be active to the present day, and to the possibility of shallow gas reserves. The $\delta^{18}O$ values change between macro-infauna vs. encrusters, indicating a warming in water temperature, reflecting glacial and post-glacial environments. The aragonite cemented sandstone has a highly variable porosity, with large vugs (open burrows and borings), smaller mouldic porosity within gastropods and bivalves and complex micro-porosity associated with acicular aragonite cements. Overall permeability was recorded at the 2.5 to 23 Darcies level, reflecting the highly variable vuggy porosity, although matrix permeability was around 100 mD and controlled by the MDAC fabric. Actual permeability will likely be controlled by the extent to which larger pores are interconnected. The sea around the Rathlin Island area contains a diverse fauna, which is worthy of future study in the context of cold seep and MDAC pavement formation.

Keywords: cold seep; $\delta^{18}O$ and $\delta^{13}C$ isotopes; aragonite; *Thalassinoides*; MDAC; porosity; permeability

1. Introduction

Methane-derived authigenic carbonate (MDAC) forms within sediments near to the seafloor, within the sulphate-methane transition zone (SMTZ), through the mixing of methane derived by thermocatalytic cracking of kerogen, or the microbial decomposition of organic material in shallower muddy sediments, interacting with SO_4^{2-} from seawater; with anaerobic oxidation of methane (AOM) and sulphate reduction by sulphate reducing bacteria (SRB's) and methane utilising archaea (Figure 2) [1,2]. Methane seep carbonates are known from around the world [3], for instance offshore Costa Rica, Norwegian Sea, Black Sea, the Mediterranean, and are diverse niche ecological refugia as well as indicators of deep, leaking hydrocarbon reserves [3]. The complex methane—AOM—sulphate reaction promotes the growth of carbonate cemented hardground pavements, which have been reported from a number of locations within the Irish Sea [2,4–12], the best three documented examples being Holden's Reefs (Tremadog Bay, offshore Wales), the Codling Fault Zone (Irish Sea, Ireland) and the Croker Carbonate Slabs (Irish Sea, Ireland) [2]. The last occurs at a water depth of 70 to 100 m, covers an area of some 500,000 m^2, and may have been a continuously active methane seep for 17,000 years [2]. MDAC phases include acicular aragonite and high-magnesium calcite, with associated pyrite [2]. Other authors have also reported high-magnesium calcite (up to 48 mol% $MgCO_3$) and dolomite from the Croker site [4,5], while the Codling Fault Zone has been described as aragonite dominated [11]. Pavements are typically relatively thin, and have commonly been exposed by local erosion and colonised by modern encrusting organisms [2]. The Croker site records MDAC with a depleted $\delta^{13}C$ of between −34 to −54‰, which indicates a thermogenic methane origin from the cracking of kerogen, with a possible Carboniferous source [1,2]. Material collected from offshore, Rathlin Island, Northern Ireland, indicates an extension of the known range of MDAC cementation within the Irish Sea area, and comes from shallower water depths than those previously described. The occurrence is herein described in terms of its composition, $\delta^{13}C$ and $\delta^{18}O$ isotopes, porosity and permeability and discussed in terms of its potential as an indicator of environmental information, as well as hydrocarbon exploration in the area and potential significance as an MDAC associated marine protected area.

2. Materials and Methods

A single block of Quaternary methane-derived authigenic carbonate (MDAC) was collected by divers, from the seafloor near Rathlin Island, County Antrim, Northern Ireland. The block was slabbed using a diamond thin sectioning saw and optically imaged (Figure 1). Some of the material was resin impregnated and made into polished thin sections. The latter, along with smaller broken surfaces were additionally imaged using a Quanta 650 FEG scanning electron microscope (SEM) (Thermo-Fisher Scientific, Waltham, Massachusetts, USA). Samples were examined uncoated and imaged in low vacuum mode utilising backscattered electrons (BSE), with both single images and larger scale montages collected [13]. Biogenic components and aragonite cement samples were analysed for $\delta^{13}C$ and $\delta^{18}O$ isotopes (Scottish Universities Environmental Research Centre (SUERC), East Kilbride), using a VG SIRA 2 triple collector, dual inlet isotope ratio mass spectrometer (VG Instruments, Crawley, West Sussex, UK): for information on the technique see Mitchell et al. [14], Parkinson et al. [15]. X-ray diffraction (XRD) analysis was also carried out (University of the West of Scotland) for carbonate mineralogy, using a Seimens D5000 X-ray powder diffraction system (Bruker Corporation, Billerica, Massachusetts, USA). A 25 mm core plug was also scanned by X-ray tomography (XRT) using an RX Easy Tom ET150 (RX Solutions, Annecy, France), for porosity, and a portable TinyPerm permeameter (New England Research Inc., White River Junction, VT, USA) was used to collect permeability data. In addition, ImageJ (open source software, Wayne Rasband, National Institutes of Health, Bethesda, MD, USA) and pore analysis tools (PAT) (Heriot-Watt University, Edinburgh, Scotland) were used to assess porosity and permeability.

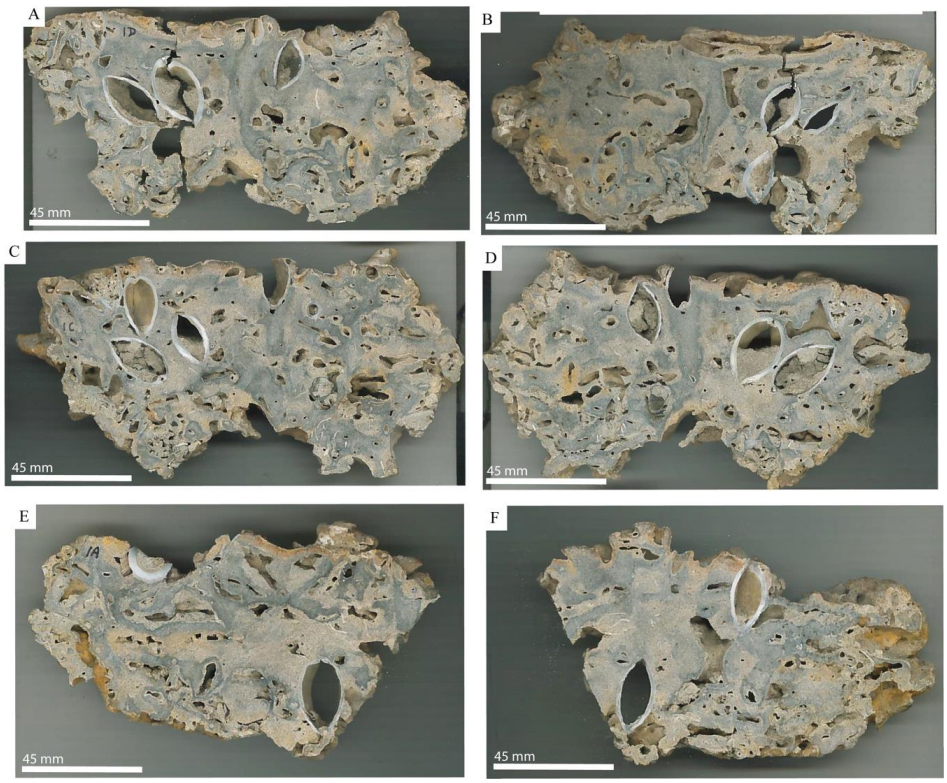

Figure 1. (**A**–**F**) Optical photographs of sawn slabs of methane-derived authigenic cement (MDAC) pavement, from the current study. Illustrating the occurrence of bivalves, boring and the patchy development of cement.

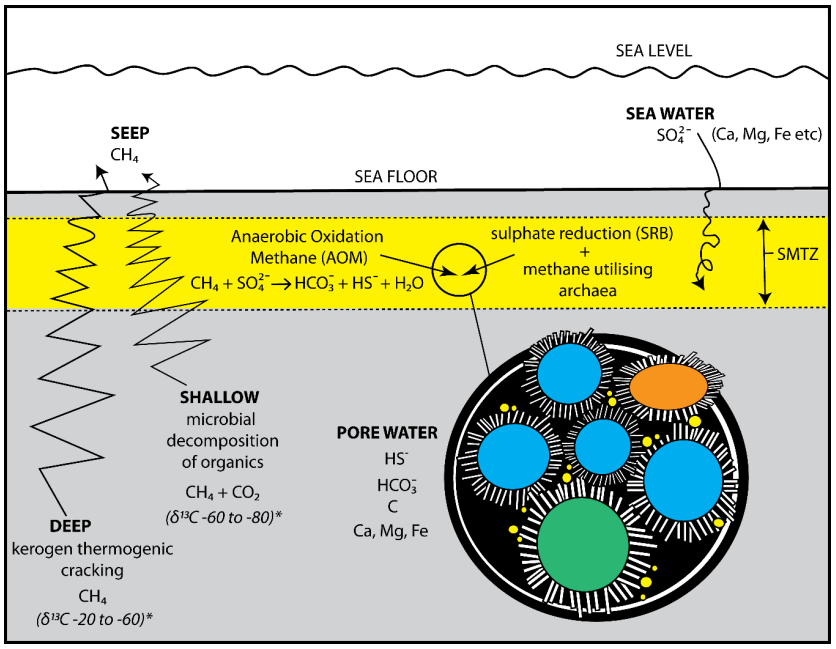

Figure 2. Processes involved in the formation of methane-derived authigenic carbonate (MDAC) and pyrites. Note $\delta^{13}C$ values for methane source from [1], * Vigneron et al. [16] put the boundary between thermogenic and microbial methane generation at −50 $\partial^{13}C$. Blue = quartz grains, orange = carbonate grains, green = feldspar grains, yellow = pyrite framboids, white = acicular aragonite. SMTZ = Sulphate-Methane Transition Zone.

3. Results

Overall, the hardground has a chaotic rubbly appearance, which is only clarified through slabbing (Figure 1) and thin sectioning of the material:

3.1. Matrix and Cement

The hardground is a mixed calcareous-siliciclastic sandstone, variably cemented by an aragonite cement. Grains are typically 100 to 300 µm in size (very fine to fine, with some medium sand), often appearing to float within a matrix of carbonate cement. Some coarse silty horizons occasionally occur, but are restricted within bivalve shells and as fills to large horizontal burrows. Smaller bicarbonate particles include echinoderm spines (Figure 3e,f), and foraminifera (Figure 4b,c). Aragonite cement comprises of blade like to acicular shaped morphology (Figure 3b–d), forming rimming cements to grains, bivalves and burrows. Pyrite framboids (~5 to 20 µm) are common (Figure 3g,h), as are also zircons (not illustrated). Porosity is highly variable (see Section 3.4).

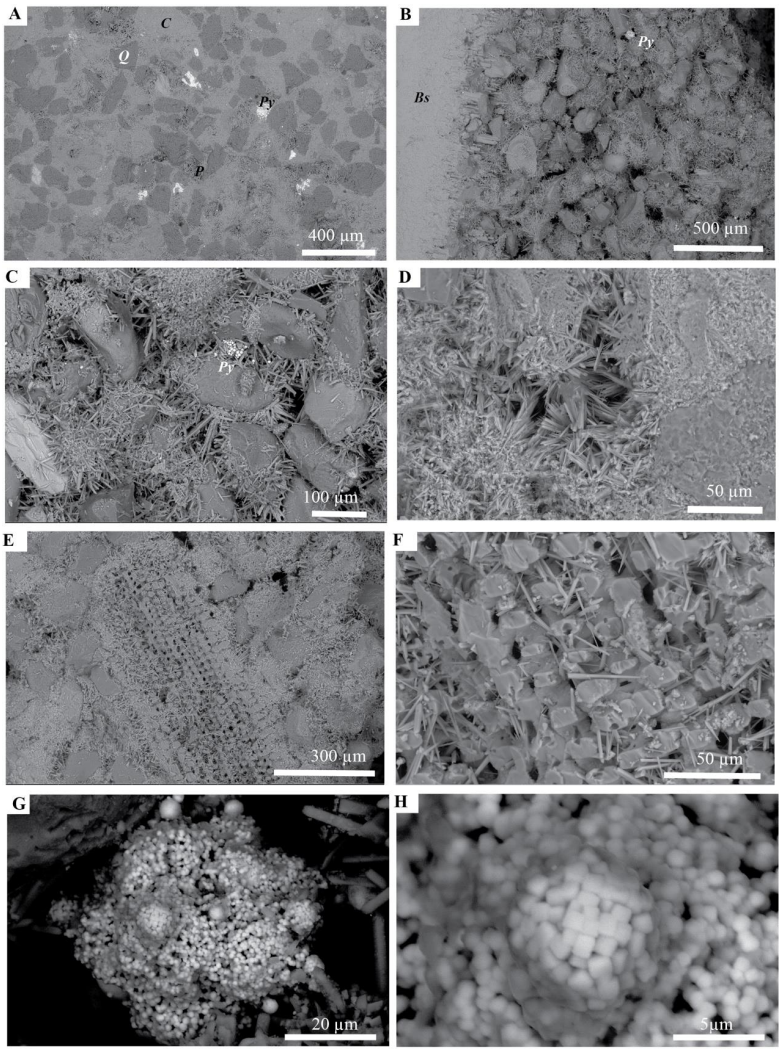

Figure 3. Backscattered electron (BSE) micrographs of hardground features and fabric. (**A**) Highly carbonate cemented area of matrix. C = carbonate particle, Q = quartz, Py = pyrite and P = more porous area, with less cement. (**B**–**D**) Increasing magnification views of typical areas with aragonite acicular cement. In (**B**), the left-hand side illustrates bivalve shell, with aragonite fringe. (**E**,**F**) Carbonate particle (echinoderm spine), with aragonite fringe. (**G**,**H**) Details of pyrite framboids, associated with organic material (darker grey).

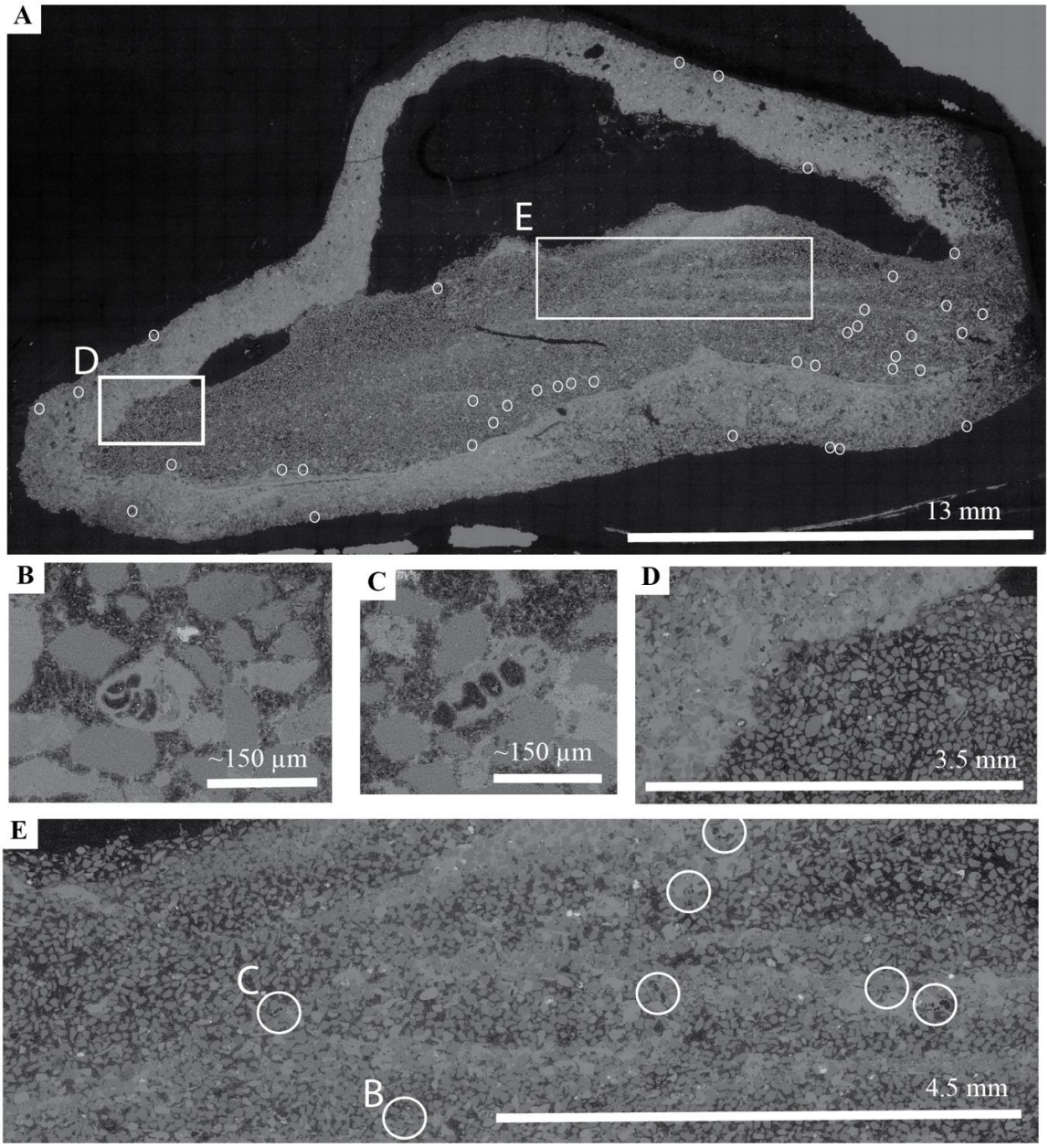

Figure 4. Backscattered electron (BSE) micrographs of hardground features and fabric. (**A**) Montage of open horizontal burrow system (*Thalassinoides*), partially infilled with sediment. Note that the burrow is surrounded by a well-cemented halo. (**B**,**C**) Foraminifera from sediment within burrow. (**D**) Detail of wall-burrow interface, illustrating stark contrast in degree of cement. (**E**) Section of sediment within burrow illustrating alternating laminae of well-cemented and poorly-cemented. Additionally, areas of pyrite (bright areas). Note in all images, pores appear black. Open circles in (**A**,**E**) represent the location of calcaceous microfossils (mostly foraminifera).

3.2. Fauna

Owing to their occurrence within the cemented hardground, no material has been taxonomically identified to species or genus level. However, the fauna is dominated by bivalves, both burrowing and boring forms with some gastropods (Figure 1), and an encrusting fauna of bryozoans, calcareous algae and calcareous worm tubes (not illustrated). Complete (intact) closed bivalves are often observed within the hardground, and are variably orientated, with no sign of a preferred life position. Foraminifera are also commonly observed within the sediment, both in SEM and XRT (Figure 4).

In addition, finger sized, horizontal, open burrows (*Thalassinoides*) have been observed (Figure 4a), although their three-dimensional morphology is not clear. The latter have their walls cemented by aragonite, and are partially infilled by repeated pulses of fine sand to coarse silty sediment which is variably carbonate cemented.

3.3. Isotopes

$\delta^{18}O$ values can be roughly subdivided into two groups, with slight overlap, with bivalves and gastropods ($\delta^{18}O$ = 1.64 to 3.33‰) and surface encrusting organisms ($\delta^{18}O$ = −0.47 to 1.74‰). It is also notable that there is no clear separation between macro-fauna pre- or post-cementation ($\delta^{18}O$ = 1.64 to 3.33‰ versus 2.14 to 2.91‰ respectively). Authigenic MDAC aragonite has the consistently highest $\delta^{18}O$ values (3 to 3.29‰), which is only matched by one of the large bivalves (Table 1).

Table 1. Composition (X-ray diffraction (XRD)), $\partial^{13}C$ ‰ V-PDB, $\partial^{18}O$ ‰ V-PDB and temperature, for biological calcite and aragonite cement from the Rathlin sample. Analytical precision ± 0.1‰. Temperature calculated based on Epstein et al. [17]: T = 16.5−4.3 δ + 0.14 δ^2; T = temperature in °C, and δ = $\delta^{18}O$ for calcite. Key: low magnesium calcite (LMC), high magnesium calcite (HMC), indeterminate (INDET).

Description	Comp (XRD)	$\partial^{13}C$ ‰ V-PDB	$\partial^{18}O$ ‰ V-PDB	T °C
Gastropod in hash at base	aragonite	−2.86	2.33	6
Large bivalve	aragonite	1.52	2.07	7
Large bivalve (convex up)	aragonite	1.23	3.33	1
Large bivalve (convex up)	aragonite	−1.46	2.45	5
Large bivalve (convex up)	LMC	−1.75	2.39	5
Burrowing bivalve	aragonite	−1.68	2.13	7
Burrowing bivalve	aragonite	−1.01	2.26	6
Burrowing bivalve	aragonite	−0.26	1.64	9
Burrowing bivalve	aragonite	−1.99	2.26	6
Burrowing bivalve	aragonite	−0.3	1.85	8
Burrowing bivalve	aragonite	−5.16	1.7	9
Burrowing bivalve	aragonite	−3.81	2.13	7
Boring bivalve	aragonite	−3.84	2.24	6
Boring bivalve	aragonite	−8.1	2.59	4
Boring bivalve	aragonite	−0.98	2.14	7
Boring bivalve	aragonite	−2.18	2.61	4
Boring bivalve	aragonite	−5.56	2.5	5
Boring bivalve	aragonite	0.39	2.22	6
Boring bivalve (large)	aragonite	−3.14	2.39	5
Boring bivalve	aragonite	−5.04	2.45	5
Boring bivalve	aragonite	−5.76	2.91	3
Boring bivalve (small)	aragonite	−2.79	2.68	4
Bryozoan (encrusting)	LMC	−0.99	0.77	13
Bryozoan (encrusting)	LMC	−3.25	1.74	9
Bryozoan (encrusting)	LMC	−2.5	1.23	11
Encrusting white algae	HMC	−5.43	0.26	15
Encrusting white algae	HMC	−4.8	−0.47	18
Annelid tube	INDET	−1.32	1.7	9
Annelid tube (*Pomatoceros*)	HMC	−1.34	−0.06	17
Cement (acicular)	aragonite	−48.99	3	2
Cement (acicular)	aragonite	−60.09	3.29	1

In terms of $\delta^{13}C$ the aragonite MDAC cement is clearly separated from all biogenic calcites (regardless of phase — aragonite, low magnesium calcite (LMC), high magnesium calcite (HMC)), with strongly negative values of −48.99 and −60.09‰, compared to values of between −8.1 to 1.52 (Table 1). The large bivalves have $\delta^{13}C$ values centered around zero, with −1.75 to 1.52‰ (Table 1). All other faunas have essentially negative $\delta^{13}C$ values, of which the boring bivalve fauna has the most depleted values (up to −8.1‰), but also records one positive value of 0.39‰ (Table 1). Nevertheless, none of the macrofauna nor encrusters can be clearly distinguished based on their $\delta^{13}C$ ranges (Figure 5c).

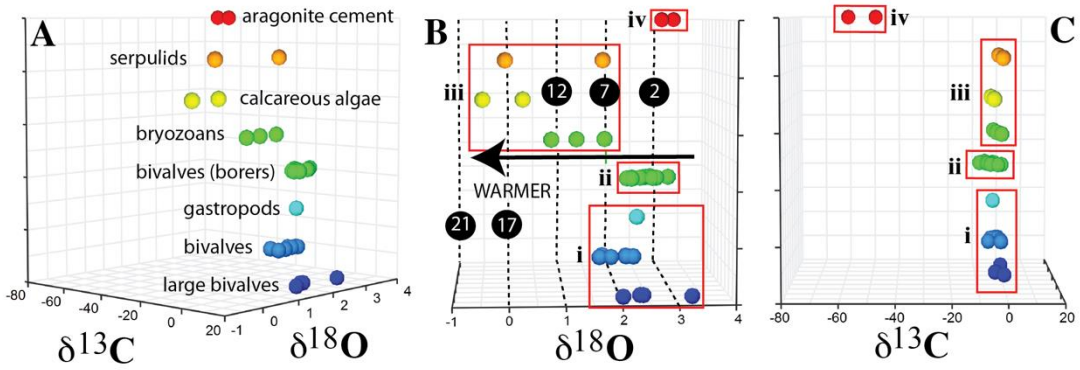

Figure 5. Plots of $\delta^{18}O$ and $\delta^{13}C$ values, for materials measured during the current study. (**A**) Three-dimensional plot of $\delta^{13}C$ versus $\delta^{18}O$, divided into individual specimen types along the *z*-axis, (**B**) as in (**A**) rotated to clearly display differences in $\delta^{18}O$ between groups, (**C**) as in (**B**) but to show $\delta^{13}C$. Key: (i) pre-hardground fauna (bivalves and gastropods); (ii) post-hardground "boring" bivalve fauna, or co-occuring bivalve fauna associated with hardground cementation; (iii) late developing encrusters (bryozoan, encrusting calcareous algae, serpulid tubes); (iv) aragonite needle-like cement. Figures in black circles = T °C after Epstein et al. [17]. Note vertical axis only used to separate the different tested groups, no scale. Temperature values for aragonite cement are not likely to be accurate (see Section 4.2.1).

3.4. Porosity and Permeability

The material examined from Rathlin is highly variable in porosity [13], with (1) variably infilled finger sized pores within open burrow systems of *Thalassinoides* (Figures 4a and 6a); (2) millimetre to centimetre scale pores of variable inclination from boring organisms into the cemented hardground (Figures 1 and 6b); (3) variably filled centimetre scale cavities within bivalves (Figures 1 and 6c); (4) normal inter-particle porosity associated with sediment infill of burrows, borings and bivalves (Figure 4d,e and Figure 6d); and (5) irregularly shaped inter-crystalline porosity between the acicular or bladed cements, which surround the sedimentary and biogenic particles (Figures 3d, 6e and 7). Porosity measured for 1214 2D slices (each ~230 mm^2) obtained from a reconstructed X-ray tomographic volume (XRT), indicates an average porosity of 14%, with a range between 6 and 28% (Figure 8). Permeability extracted from the XRT reconstruction using the PAT software gives values between 2515 and 23,307 mD, depending on the direction in which the permeability is calculated (Table 2). However, direct measurements taken for sampled areas of the cemented matrix records permeability with an average of 100 mD (Figure 9, Table 2).

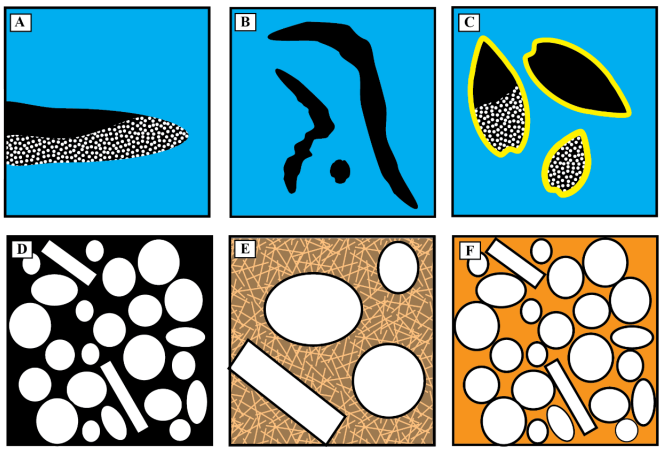

Figure 6. Schematic cartoons of the variability in porosity. (**A**–**C**) macro-porosity, from (**A**) Horizontal burrows (*Thalassinoides*), (**B**) variably shaped/oriented borings, (**C**) porosity within bivalves. (**D**–**F**) variability in micro-porosity, with end members of (**D**) no cement, inter-particle porosity well-developed, (**F**) up to 100% cement, no inter-particle porosity; (**E**) partially cemented with bladed and acicular aragonite, resulting in complex irregular inter-crystalline porosity. Note that blue areas of matrix in (**A**–**C**) are often well-cemented as in (**F**), while sediment within macro pores illustrated in (**A**–**C**), typically have porosity as in (**D**,**E**), with thin well cemented laminae (**F**) (Figure 4e). Additionally, burrows often surrounded/demarcated by pore-occluding cement, as in (**F**).

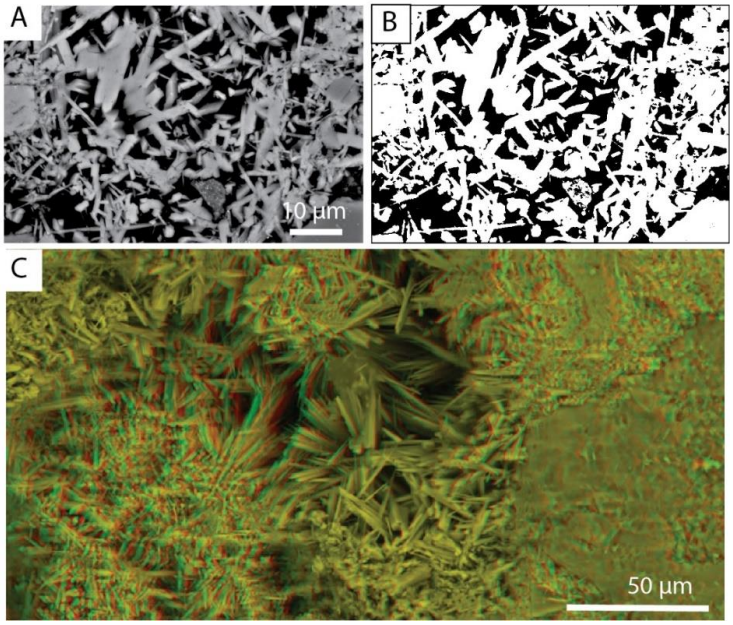

Figure 7. Illustration of complex pore morphology associated with acicular cements. (**A**) Scanning electron microscope (SEM) image, (**B**) binarised image of (**A**) for porosity (black), porosity = 62%, signifying that much of the pore space is open, but highly compartmentalised and baffled. Pores are difficult to model in terms of permeability using digital rock modelling (DRM) techniques, as they do not conform to the standard spherical pore models commonly used. (**C**) Three-dimensional stereo image, illustrating the complexity of pore spaces in three dimensions (requires green-red stereo glasses).

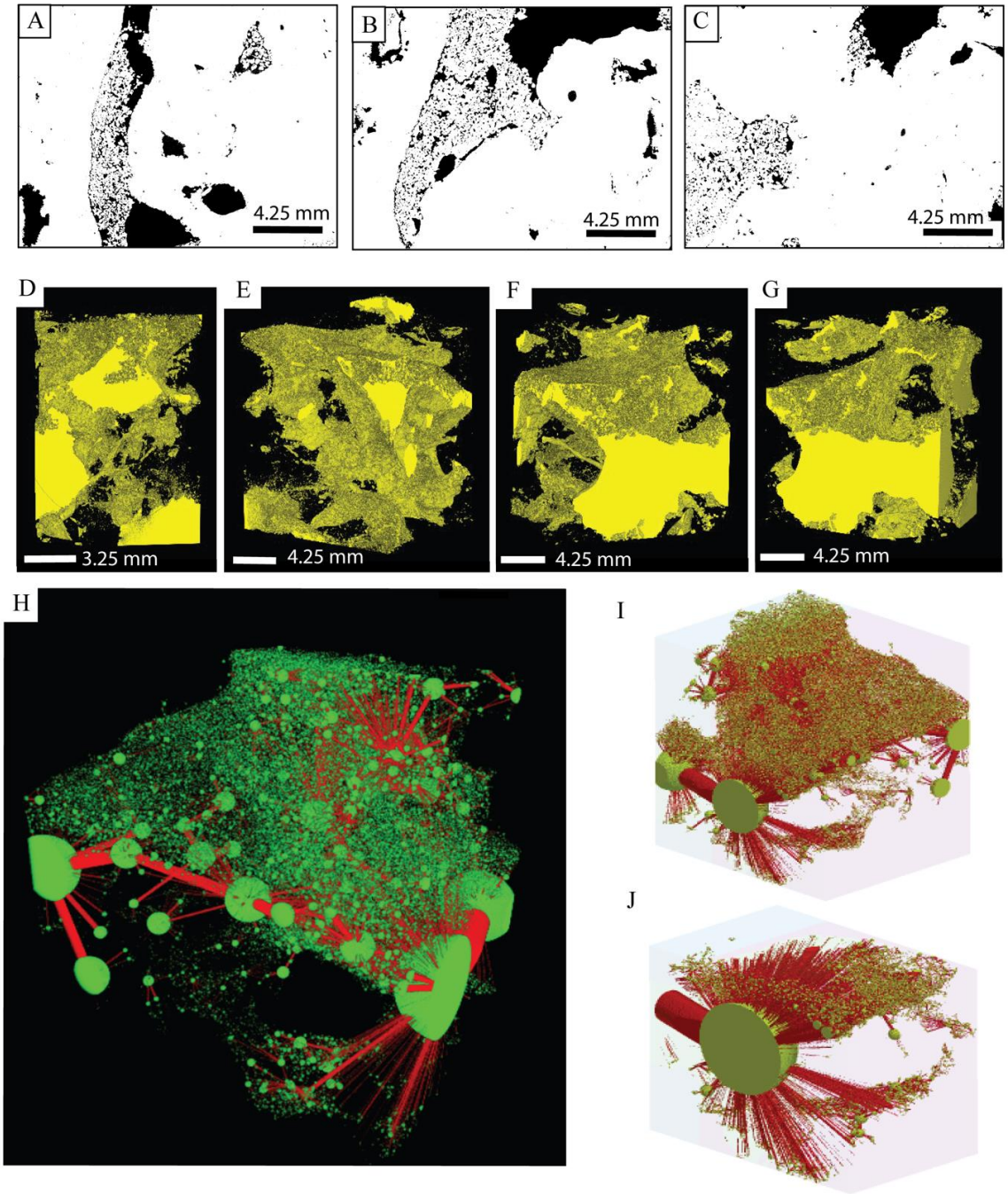

Figure 8. (**A**–**C**) Binarised slices through X-ray tomographic reconstruction of the Rathlin sample, black = pores, white = solid. Images 1341 by 1020 pixels, ~13 μm per pixel. (**D**–**G**) 3D reconstructions of porosity (yellow), at various rotations, from the same scan as in (**A**–**C**). Full movie of 3D reconstruction available in Supplementary Materials. (**H**–**J**) Ball and stick models of pore connectivity used to model permeability; balls representing pores, and sticks pore throats, with size indicating relative size. (**H**,**I**) overviews of whole sample at different orientations, (**J**) enlargement of (**I**) illustrating connection of small pores to the larger pore system.

Table 2. Permeability values recorded using X-ray tomography (XRT) in the X, Y and Z directions, and TinyPerm from points 1–6 in Figure 9.

XRT	Direction	X		Y		Z	
	Permeability (mD)	2515		23,307		11,732	
TinyPerm	**Sample point #**	**1**	**2**	**3**	**4**	**5**	**6**
	Permeability (mD)	98.88	94.21	96.46	94.09	96.26	122.2

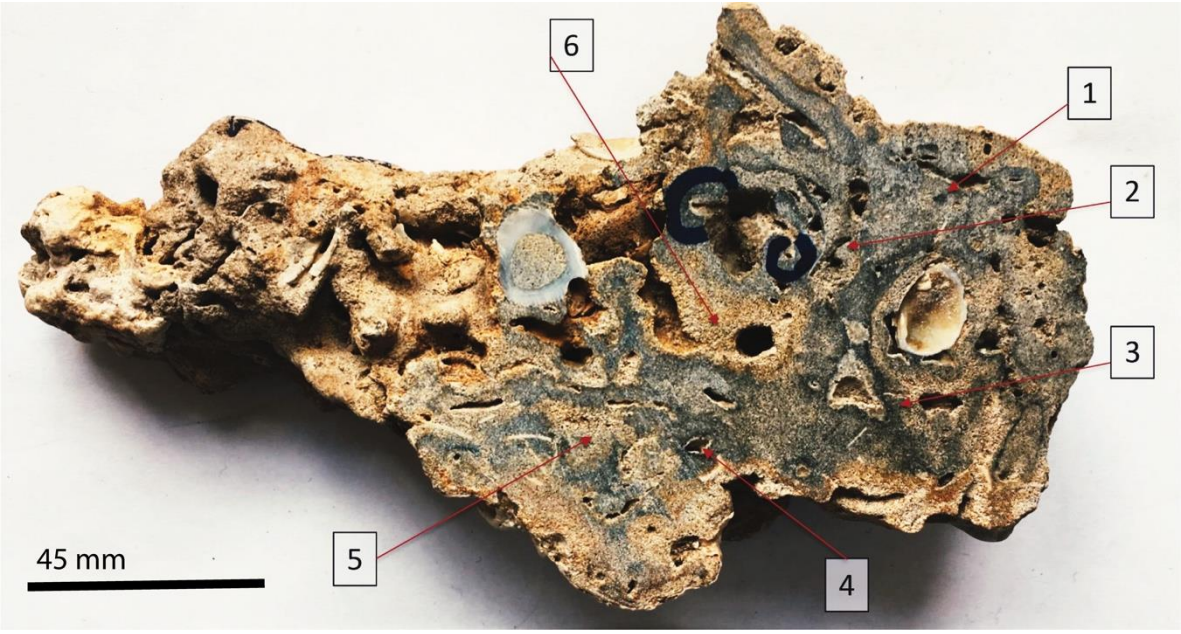

Figure 9. Permeability measured (through air injected decay pressure) from the matrix of sample. Individual permeability values given in Table 2. Average permeability 100.35 mD.

4. Discussion

Material referred to as boring bivalves is so labelled on the basis that they occurred loose and 'imprisoned' within borings. Another possible interpretation is that such material represents a post-depositional fauna living within, or washed/trapped within, open vertical burrows formed just prior to cementation. Other bivalves either occurred as pairs of closed valves, or as large singular valves, both enclosed within sediment. The co-associated closed valves occur in a variety of orientations, suggesting that they are a death-assemblage deposited after a storm event. The orientation of the block is unknown, however, the large single valves are all the same way up, and occur on just one side of the block. Given the size of the valves and the storm deposited postulated origin, these are likely to occur on the base of the bed, and are therefore concave-up.

Finger sized open horizontal burrows, partially infilled by repeated ingress of silty sediment may represent *Thalassinoides*, or similar horizontal networks of open living burrows. Lack of sample material prevents more detailed analysis, although Figure 4a appears to have a potential vertical entrance burrow connected to a horizontal section of burrow.

4.1. Comparison with Other MDAC Sites

Similar hardground pavements are also seen from the Quaternary of the North Irish Sea Basin (but generally in deeper water), Holden's Reefs, the Codling Fault Zone and the Croker Carbonate Slabs. These pavements also have acicular aragonite needles with depleted $\delta^{13}C$, and many also typically contain dolomite, non-ideal dolomite, or very high magnesium calcite [2,4,5,11]. The Codling Fault Zone is the most similar to the Rathlin material in terms of its petrography, being well cemented with acicular aragonite of a similar nature to that observed and illustrated herein [8], also containing pyrite

framboids, but no Mg enriched forms of calcite. The Codling Fault Zone MDAC deposits are also closely associated with a major fault complex, as is the Rathlin MDAC (Tow Valley Fault), which may have acted as pathways for methane migration. The other Irish Sea MDAC pavements also have similar ∂^{13}C depleted values of −33‰ (Holden's Reefs), −41 to −46‰ (Codling Fault Zone) and −34 to −54‰ (Croker Carbonate Slabs) [2,8], but are in general consistently lower than that of the Rathlin samples. The other Irish Sea areas clearly have ∂^{13}C values that fall within the range associated with thermogenically generated methane [1,16], with which they have commonly been cited [2,8]. Acicular aragonite crystals have also previously been recorded filling burrows, with depleted δ^{13}C (−43.59 to −54.54‰) from localised cold seep mounds from the Pliocene of central Japan [18]. Finally, Kinnaman et al. [19] investigated shallow water (10 m deep) carbonate cemented sands from the Brian Seep, Santa Barbara, from the AOM of a thermogenically sourced methane (∂^{13}C−43‰). Although similar in many respects to the Rathlin material, the carbonate from the Brian Seep comprises of high magnesium calcite and forms carbonate concretions [19], rather than more widespread acicular aragonite cement.

4.2. Significance of Isotopes $\delta^{18}O$ and $\delta^{13}C$

4.2.1. Significance of ∂^{18}O Distributions:

Many biominerals have ^{18}O values that precipitate in equilibrium with the isotopic composition of the host marine water, which is generally the case for calcite within bivalves [20], bryozoa [21,22], encrusting calcareous algae [23] and serpulid tubes [24]. As noted earlier, a separation in δ^{18}O values between the macrofauna (bivalves and gastropod) and encrusting fauna can be noted with a small degree of overlap between ∂^{18}O 1.64 and 1.74‰. This equates to a temperature of 9 °C, suggesting a relative increase in water temperature between the two groups, with the macrofauna reflecting temperatures between 1 to 9 °C, while the encrusters record between 9 and 18 °C (Table 1, Figure 5b). This fits with an increase in water temperature since the formation of the hard ground in the Quaternary. As the sea warmed, additional encrusting organisms colonised the substrate. Encrustation may range from recent to modern, with the latter supported by comparison with monthly average sea water temperatures of 8–14 °C recorded at nearby Ballycastle [25]. This would agree with the findings of Judd et al. [2] for encrusters on the Croker Carbonate Slabs.

In addition, many of the bivalves interpreted as borers have a more positive δ^{18}O signature, in comparison to the burrowing bivalves and bulk of the isolated large single bivalve valves (Table 1), suggesting the possibility of slightly cooler palaeo-water temperatures after formation of the hardground. Unlike other boring fauna such as from the Croker Carbonate Slabs, the similarity in temperature between all forms of bivalves, and the separation in terms of δ^{18}O (temperature) from the encrusting fauna is indicative that at least some proportion of observed borings occurred soon after hardground formation. The wide range of temperature values interpreted from the large isolated single bivalve valves (minimum temperature 1 °C, maximum 7 °C) may reflect a longer range of depositional periods, some commensurate with cooling during the glacial maximum.

Oxygen isotopes in bivalves can also be influenced by salinity, becoming increasingly lower in δ^{18}O [26], and can vary with age and shell layer [26,27]. The relationship with shell ultrastructure was not taken into consideration from the current samples, and may, in part, explain some of the variability recorded within the different bivalve groups. No evidence was noted to suggest that the bivalves were non-marine, or subject to lower salinities, with no negative δ^{18}O excursions, and calcareous microfossils within the matrix material of the hardground are suggestive of normal marine conditions.

The δ^{18}O values for the aragonite cementing phase records amongst the most enriched values (3 and 3.29‰), which equate to a temperature of between 1 and 2 degrees. Assuming that these values are in equilibrium with seawater, this is likely to indicate that hardground formation was at its zenith during the height of glacial development. However, a number of previous authors [2,11,28] have pointed out that enrichment in δ^{18}O from waters rising from gas sources, or from the dissociation of gas hydrates, mixing with seawater within pores can skew the results (resulting in cooler values than

otherwise expected). This is highly likely, with similar but more $\delta^{18}O$ enriched values of + 3.9 to + 4.8‰ recorded from aragonite crusts associated with methane seeps from deep-sea fans of the Congo, related to altered pore water chemistry caused by gas hydrate dissociation [29].

4.2.2. Trends $\partial^{13}C$ Isotopes

The $\delta^{13}C$ isotopes recorded from the acicular aragonite cement are strongly depleted. Depletion in $\delta^{13}C$ can have a number of sources, from the production of methane through microbial breakdown of organic matter in sediment, to thermogenic release of methane during kerogen 'cracking' [1,16]. Isotopically heavier values (−20 to −60‰) were recognised by Judd [1] as being of a more thermogenic methane origin, while the more $\delta^{13}C$ depleted (−60 to −80‰) being indicative of biogenic (microbially) sourced methane. Vigneron et al. [16], although generally in agreement with this placed the boundary between thermogenic and microbially derived methane at −50‰, with an upper limit for biogenic methane at −110‰. For the majority of Irish Sea MDAC pavements, this does not pose a major problem, as, in either case, most would fall into the thermogenically derived window (see Section 4.1). However, for the Croker Carbonate Slabs (−34 to −54‰) and the Rathlin MDAC (−49 to −60‰), it is likely that for the Croker Carbonate Slabs the cement may have a mixed methane source, while that of Rathlin may be substantially more microbially derived. Stolper et al. [30] indicated that isotopic and compositional parameters may not be enough to clearly differentiate methane source within cold seeps, advocating the use of clumped isotope studies, which benefit also by providing data on temperature during methane generation. Even so, for high rates of methane production, not in equilibrium with the temperature at the time of methane production, some ambiguity in diagnosing the methane source still exists [30]. Nevertheless, whatever the source of methane, there is general agreement that MDAC formation would have occurred near the sediment surface, within the sulphate-methane transition zone (SMTZ), mediated through the biological anaerobic oxidation of methane (see Figure 2) [1,2]. Work on lipids from those microbiota responsible for anaerobic oxidation of methane (AOM), contained within MDAC, characteristically shows extreme depletion in $\delta^{13}C$, with −137 to −93‰ $\delta^{13}C$ [31], as low as −127‰ $\delta^{13}C$ [32] and at least −100‰ from MDAC associated lipids of the North Sea [33]. In addition, Himmler et al. [32] also recorded $\delta^{13}C$ values of as low as −101‰ from biomarkers of sulphate reducing bacteria. Microbial activity during AOM is well known to have a fractionation effect for $\delta^{13}C$ [31,34], consequentially offsetting $\delta^{13}C_{methane}$ by approximately 20 to 60‰ [31]. This effect was clearly illustrated by Himmler et al. [32], with $\delta^{13}C_{carbonate}$ −54.6‰, with actual recorded $\delta^{13}C_{methane}$ values of −70.3 to −66.7‰. Therefore, given the recorded $\delta^{13}C_{aragonite}$ of −49 to −60‰ from the Rathlin aragonite MDAC cement, it appears more plausible that, in this case, the source for methane is of a shallow microbially derived form. The latter may at least in part also be the case for the Croker Carbonate Slabs MDAC.

The majority of the fauna present within the sample are depleted in $\delta^{13}C$ (Table 1). The $\delta^{13}C$ of marine bivalves is commonly neutral to slightly positive, with Jurassic examples recorded with values of 0.3 to 5.1 [35]. However, it has been shown that fluviatile bivalves can have $\delta^{13}C$ values in the range of −13.7 to −6‰ [36], Leng and Lewis [26] reporting similar values of between −12 and −8 for freshwater *Unio* bivalves, and similar recorded for *Mytilus edulis* from tidal zones [37]. Such negative values are likely a result of the influence of depletion within the filtered food source [36,37]. It is therefore plausible that the recorded negative values within bivalve shells from the present study reflect the nature of their food source, in itself influenced by the continuous presence of the methane cold seep. Fluctuations in $\delta^{13}C$ values representing differences in food source, or possibly seasonal variations recorded within the shell.

Bryozoans can display a range of $\delta^{13}C$ values, with Key et al. [38], recording values of between −2.2 and 2.5‰ from the Miocene, in which depletion in $\delta^{13}C$ was attributed to the upwelling of nutrient-rich waters. Although this may be the case at Rathlin, which does possess a rich and diverse marine fauna [39], this may, in part, reflect the continued presence of the cold seep around the Rathlin area.

Williams et al. [40], illustrated that coralline algae hold records of depletion in $\delta^{13}C$ within surface seawater, brought about by changes in the dissolved inorganic carbon content. Therefore, it is possible that the depletion in $\delta^{13}C$ (−5.43, −4.8‰), recorded herein, may be due to upwelling, or possibly anthropogenic influences, but, given the relatively large surface area to volume ratio of the white coralline algae, and their encrustation on the MDAC surface, perhaps more reasonably bears witness to the continued emission of methane through the cold seep.

Doss [41] illustrated an example where $\delta^{13}C$ depletion in serpulid tubes occurred under hyposaline (abnormally low salinity) conditions compared to fully marine, and other authors have also shown that freshwater annelid tubes can be highly depleted in $\delta^{13}C$ [42]. The depletion herein is not high enough to indicate freshwater dilution. The $\delta^{13}C$ and $\delta^{18}O$ values for the annelid tubes are not that dissimilar to other normal marine annelid tubes [43], although the slight depletion in $\delta^{13}C$ is likely to also be related to continued activity of the cold seep.

Judd et al. [2] reported $\delta^{13}C$ values from the Croker Carbonate Slabs, for serpulids, bryzoans and shells of between −1.46 to +1.39‰, consistent with normal marine carbonates, although noting that some biogenic material was depleted with $\delta^{13}C$ values of approximately −12‰. This was interpreted as a mixture of MDAC and normal seawater values, and hence reflects the influence of the active methane seep. Therefore, it is likely that as indicated, many of the boring bivalves ($\delta^{13}C$ −3 to −6‰), some encrusting bryozoans (around −3‰), the encrusting calcareous algae (−5‰) and possibly the recorded annelid tubes (around −1.30‰) from the Rathlin MDAC location are also witnessing growth during active methane seepage and growth of the MDAC material.

4.3. Significance of Porosity and Permeability

Although areas with inter-particulate and inter-crystalline micro-porosity are common, permeability data suggest that flow through this matrix material may be limited to the order of 100 mD. X-ray tomographic reconstructions of the hardground (Figure 8), illustrates the complex relationships between the different styles of observed pores and a high likelihood of connectivity between the macro-pores (open burrows—'*Thalassinoides*'—borings and large open spaces between paired bivalve shells), strongly suggesting higher levels of permeability in certain situations; which will be further supplemented by inflow from micro-pores within the matrix (inter-particle and inter-crystalline pores). The latter pore type is too small to easily and accurately measure by XRT, and would require 3D digital rock modelling (DRM) methods, utilising higher resolution SEM images. Although such techniques are not uncommon [44–46], the unusual pore shape and complex three-dimensional structure of the MDAC aragonite cements and their associated pore spaces (Figure 7), would make it difficult to model permeability using traditional DRM techniques. Nevertheless, future analysis would greatly benefit the understanding of the detailed three-dimensional geometry and flow properties of these unusual cements. However, as indicated, permeability modelling of the whole rock XRT reconstruction, which takes into account the larger observed macro-pores and a range of the simpler inter-particle micro-pores, indicates permeability levels in the tens of Darcies (Table 2). As would be expected, flow through the macro-pores is highly variable, depending on the orientation and connectivity of such structures. The hardground would be expected to act similar to microporous materials within a fractured rock system, having at least both dual porosity and permeability. Zwicker et al. [47] discussed the possibility that the burrows of callianassid decapods (*Sponeliomorpha*, *Ophiomorpha* and *Thalassinoides*) may act as conduits in the upper parts of methane-seep deposits, thus assisting in the distribution of mineralising fluids and gasses, and the continuation of AOM mediated cementation. Likewise, the observed '*Thalassinoides*' burrows recorded from the Rathlin material could have provided a similar function. Haas et al. [29] illustrate similar material to '*Thalassinoides*', which were also lined with aragonite, but represent non-biological gas flow conduits, associated with higher gas flow rates. Therefore, it is possible that the Rathlin '*Thalassinoides*' have a similar non-biological origin, instead being formed due to high gas flow rates. In either case, such structures will greatly increase connectivity between areas of subsurface AOM carbonate formation and the seafloor [29,47]. The occurrence of aragonite

within pipework/*Thalassinoides*, which are interpreted as conduits for the free flow of methane is of particular interest as Judd et al. [2] postulated that areas with Mg calcite within the Croker Carbonate Slabs represented parts of a free flowing system, while aragonite formed when pores were occluded, resulting in slower diffusion of methane through the sediment. Clearly this is at odds with observations from other MDAC systems, indicating that the form of calcite precipitation (Mg calcite versus aragonite) must depend on more than a single parameter such as flow rate.

4.4. Hydrocarbon Potential

The area around Rathlin Island (Rathlin Basin), and the closely associated North Channel, have received interest in terms of hydrocarbon exploration [48,49]. In terms of the Rathlin area, good reservoir potential exists within Carboniferous age sandstones and the Triassic Sherwood Sandstone Group, with hydrocarbon sourced from Carboniferous coals and organic-rich sediments [48]. However, no clear seals have been identified, with the absence of the Mercia Mudstone Group halite deposits which act as seals in the nearby Larne Basin, leaving only potential localised seals within the Carboniferous aged sequence [48]. Nevertheless, drilling within the Rathlin Basin area, has indicated a number of oil shows within cored materials, and the presence of seeps [48]. The major Tow Valley Fault, which passes to the east of Rathlin Island, which juxtaposes Pre-Cambrian meta sediments against post-Triassic strata [49], may act as a conduit for the migration of shallow methane and the formation of cold methane seeps. Further investigation on the origin of methane (microbial versus kerogen cracking), confirmation on the presence and extent of MDAC pavements (in the Rathlin area), and evidence of continued methane cold seeps, may help to further constrain hydrocarbon potential in the Rathlin Basin and surrounding area. Although the recorded $\delta^{13}C$ values of −49 to −60‰ for the Rathlin MDAC are most likely indicative of microbial, rather than thermogenic, methane (see Section 4.2.2), these only represent two samples. Further investigation and analysis may indicate a wider range of values similar to many of the other Irish Sea MDAC pavements (see Section 4.1), and the possibility of a more mixed methane source.

4.5. Conservation Habitat

Twenty-seven cold seep MDAC marine protected areas (MPA's) from shallow water (less than 200 m) have been designated in European waters, which are important habitats for conservation [50]. The Croker Carbonate Slabs area was chosen by Noble-James et al. [50] to characterise such shallow water MDAC pavements, and its relatively unimpacted associated biological community. The waters surrounding Rathlin Island are already recognised as an important biological conservation area, with a rich and diverse fauna [39]. The shallower water depth of the Rathlin MDAC make this location a potentially important site for additional research of such important habitats. This would allow for the assessment of the current state of cold seep activity in the Rathlin area, the abundance and relative distribution of MDAC, as well as the relationship with the diverse associated fauna.

5. Conclusions

Our analysis of this methane-derived authigenic carbonate (MDAC) cemented sandstone off the coast of Rathlin Island extends the known range of this process within the Irish Sea. Furthermore, we demonstrated the complex interaction of methane expulsion, sulphur-reduction and a palimpsest of faunal inhabitation that will add to the understanding of MDAC [51]. Further work would ideally confirm whether this is an extensive pavement, or patchy in extent. In terms of $\delta^{13}C$ isotopes, the Rathlin MDAC appears to differ from other known areas in the Irish Sea, having a signature that suggests a shallower microbially derived source for methane. Nevertheless, further investigation would be helpful in confirming this difference, and an assessment for potential gas exploration in the Rathlin Basin area.

The Rathlin MDAC hardground is similar to others recorded from the Irish Sea, although apparently lacking high-magnesium calcite or dolomite cements, with only aragonite being developed—therefore

being more similar to the Codling Fault Zone than the Croker Carbonate Slabs. Although much of the encrusting fauna may be modern, as is the likely case for those observed at the Croker Carbonate Slabs location [2], at least some of the boring at Rathlin appears to be related to Quaternary activity, shortly after hardground formation. These differences may be due to the shallower depth of the Rathlin material.

MDAC has a complex structure with consequentially variable porosity, with macro-porosity related to burrows, borings, and cavities within bivalves, and inter-particle and inter-crystalline micro-porosity variably developed dependant on the level of cementation. The matrix has a permeability of around 100 mD, although flow through the larger pores has been modelled in the range of 2.5 to 23 Darcies. Actual permeability in the field will be controlled by the connectivity and orientation of the larger more vuggy pores, and the extent of MDAC cementation.

Interest in MDAC pavements and their associated fauna as important MPA's, suggests that the Rathlin MDAC could play an important role in such studies, in conjunction with on-going investigations of other areas such as the Croker Carbonate Slabs.

Supplementary Materials: Supplementary material can be found at https://doi.org/10.5281/zenodo.3826973.

Author Contributions: Conceptualisation, J.B.; methodology, J.B.; formal analysis, J.B., T.D.; software, Z.J.; investigation, J.B.; resources, J.B., T.D., Z.J., H.L., A.R.; writing—original draft preparation, J.B., H.L., A.R., Z.J.; writing—review and editing, J.B., H.L., A.R., Z.J. All authors have read and agreed to the published version of the manuscript.

Funding: This research received no external funding.

Acknowledgments: Many thanks to the divers who collected the samples from the seabed, and Andrew Jeram (Ulster Museum) without which this work could not have happened. We also gratefully appreciate the work of the staff (1995) at the Scottish Universities Environmental Research Centre, East Kilbride (Kirsten Ross and Anthony Fallick), who carried out the isotope analysis. Gordon Curry and Anthony Fallick are thanked for encouragement and discussion. Also, we would like to acknowledge the Digital Imaging Hub at Heriot-Watt University for the opportunity to perform both scanning electron microscopy and X-ray tomography. Jennifer McKinley (Queen's University, Belfast) kindly allowed use of the TinyPerm permeameter.

Conflicts of Interest: The authors declare no conflict of interest.

References

1. Judd, A.G. *Pock Marks in the UK Sector of the North Sea*; Technical Report TR_002; UK Department of Trade and Industry: London, UK, 2001.
2. Judd, A.; Noble-James, T.; Golding, N.; Eggett, A.; Diesing, M.; Clare, D.; Silburn, B.; Duncan, G.; Field, L.; Milodowski, A. The Croker Carbonate Slabs: Extensive methane-derived authigenic carbonate in the Irish Sea—Nature, origin, longevity and environmental significance. *Geo-Mar. Lett.* **2019**, 1–16. [CrossRef]
3. Loyd, S.J.; Sample, J.; Tripatic, R.E.; Defliese, W.F.; Brooks, K.; Hovland, M.; Torres, M.; Marlow, J.; Hancock, L.G.; Martin, R.; et al. Methane seep carbonates yield clumped isotope signatures out of equilibrium with formation temperatures. *Nat. Commun.* **2016**, *7*, 12274. [CrossRef]
4. Field, L.P.; Milodowski, A.E.; Wagner, D.; Sloane, H.; Leng, M.J.; Marriott, A.L. *Mineralogy, Petrography and Stable Isotope Study of Methane-Derived Authigenic Carbonate Slabs, CEND 23/25 Survey, Part 2*; Land, Soil and coast Programme Commissioned Report CR/16/164; British Geological Survey: Nottingham, UK, 2016.
5. Field, L.P.; Milodowski, A.E.; Wagner, D.; Sloane, H.; Leng, M.J.; Marriott, A.L. *Mineralogy, Petrography and Stable Isotope Study of Methane-Derived Authigenic Carbonate Slabs, CEND 23/25 Survey, Part 1*; Land, Soil and coast Programme Commissioned Report CR/16/164; British Geological Survey: Nottingham, UK, 2016.
6. Field, L.P.; Sahy, D.; Millar, I.; Milodowski, A.E. *Analysis of Methane-Derived Authigenic Carbonates (MDAC) from the Croker Carbonate Slab, CEND 23/25 Survey. Stage 2 Radiometric Dating*; Land, Soil and Coast Programme Commissioned Report CR/17/028; British Geological Survey: Nottingham, UK, 2017.
7. Judd, A.G. *The Distribution and Extent of Methane-Derived Authigenic Carbonate*; DTI Strategic Environmental Assessment, Area 6 (SEA6); Department of Trade and Industry: London, UK, 2005; p. 69.
8. Judd, A.; Croker, P.; Tizzard, L.; Voisey, C. Extensive methan-derived authigenic carbonates in the Irish Sea. *Geo-Mar. Lett.* **2007**, *27*, 259–267. [CrossRef]

9. Milodowski, A.E.; Lacinska, A.; Sloane, H. *Petrography and Stable Isotope Geochemistry of Samples of Methane-Derived Authigenic Carbonates (MDAC) from the Mid Irish Sea*; British Geological Survey Commissioned Report CR/09/051; British Geological Survey: Nottingham, UK, 2009.
10. Whomersley, P.; Wilson, C.; Clements, A.; Brown, C.; Lang, D.; Leslie, A.; Limpenny, D. *Understanding the Marine Environment—Seabed Habitat Investigations of Submarine Structures in the Mid Irish Sea and Solan Bank Area of Search (AoS), JNCC Report no 430*; Joint Nature Conservation Committee: Peterborough, UK, 2010.
11. O'Reilly, S.S.; Hryniewicz, K.; Little, C.T.S.; Monteys, X.; Szpak, M.T.; Murphy, B.T.; Jordan, S.F.; Allen, C.C.R.; Kelleher, B.P. Shallow water methane-derived authigenic carbonate mounds at the Codling Fault Zone, western Irish Sea. *Mar. Geol.* **2014**, *357*, 139–150. [CrossRef]
12. JNNC. *Offshore Special Area of Conservation: Croker Carbonate Slabs*; SAC Selection Assessment Document Version 5.0 (5 September 2012); JNNC: Visakhapatnam, India, 2012; p. 18.
13. Buckman, J.; Bankole, S.; Zihms, S.; Lewis, M.H.; Couples, G.D.; Corbett, P.W.M. Quantifying porosity through automated image collection and batch image processing: Case study of three carbonates and an aragonite cemented sandstone. *Geosciences* **2017**, *7*, 70. [CrossRef]
14. Mitchell, L.; Curry, G.B.; Fallick, A.E. Stable-isotope and amino acid profiles of the New Zealand giant Pliocene oyster Crussostreu ingens. *Lethaia* **1995**, *28*, 237–243. [CrossRef]
15. Parkinson, D.; Curry, G.B.; Cusack, M.; Fallick, A.E. Shell structure, patterns and trends of oxygen and carbon stable isotopes in modern brachiopod shells. *Chem. Geol.* **2005**, *219*, 193–235. [CrossRef]
16. Vigneron, A.; Bishop, A.; Alsop, E.B.; Hull, K.; Rhodes, I.; Hendricks, R.; Head, I.M.; Tsesmetzis, N. Microbial and isotopic evidence for methane cycling in hydrocarbon-containing groundwater from the Pennsylvanian region. *Front. Microbiol.* **2017**, *8*, 289. [CrossRef]
17. Epstein, S.; Buchsbaum, R.; Lowenstam, H.; Urey, H. Revised carbonate-water isotopic temperature scale. *Geol. Soc. Am. Bull.* **1953**, *64*, 1315–1325. [CrossRef]
18. Nobuhara, T. Cold seep carbonate mounds with Vesicomya (Calyptogena) kawamurai (Bivalvia: Vesicomyidae) in slope-mud fades of the Pliocene forearc basin of the Sagara-Kakegawa area, central Japan. *Paleontol. Res.* **2003**, *7*, 313–328. [CrossRef]
19. Kinnaman, F.S.; Kimball, J.B.; Busso, L.; Birgel, D.; Ding, H.; Hinricks, K.; Valentine, L. Gas flux and carbonate occurrence at a shallow seep of thermogenic natural gas. *Geo-Mar. Lett.* **2010**, *30*, 355–365. [CrossRef]
20. Hui, Y.; Jie, C.; Jun, X. A review on bivalve shell, a tool for reconstruction of paleo-climate and paleo-environment. *Chin. J. Geochem.* **2014**, *33*, 310–315.
21. Machiyama, H.; Yamada, T.; Kaneko, N.; Iryu, Y.; Odawara, K.; Asami, R.; Matsuda, H.; Mawatari, S.F.; Bone, Y.; James, N.P. Carbon and oxygen isotopes of cool-water bryozoans from the Great Australian Bight and their paleoenvironmental significance. In *Ocean Drilling Program, Scientific Results Volume 182*; Hine, A.C., Feary, D.A., Malone, M.J., Eds.; International Ocean Discovery Program (IODP): College Station, TX, USA, 2003; Volume 182, pp. 1–29. Available online: http://www-odp.tamu.edu/publications/182_SR/007/007.htm (accessed on 2 July 2020).
22. Smith, A.M.; Nelson, C.S.; Key, M.M., Jr.; Patterson, W.P. Stable isotope values in modern bryozoan carbonate from New Zealand and implications for paleoenvironmental interpretation. *New Zealand J. Geol. Geophys.* **2004**, *47*, 809–821. [CrossRef]
23. McCoy, S.J.; Kamenos, N.A. Coralline algae (rhodophyta) in a changing world: Integrating ecological, physiological, and geochemical responses to global change. *J. Phycol.* **2015**, *51*, 6–24. [CrossRef] [PubMed]
24. Lowenstam, H.A.; Weiner, S. *On Biomineralization*; Oxford University Press: Oxford, UK, 1989; p. 336.
25. Ballycastle Sea Temperature. Available online: https://www.seatemperature.org/europe/united-kingdom/ballycastle.htm (accessed on 2 July 2020).
26. Leng, M.J.; Lewis, J.P. Oxygen isotopes in Molluscan shell: Applications in environmental archaeology. *Environ. Archaeol.* **2016**, *21*, 295–306. [CrossRef]
27. Hahn, S.; Rodolfo-Metalpa, R.; Griesshaber, E.; Schmahl, W.W.; Buhl, D.; Hall-Spencer, J.M.; Baggini, C.; Fehr, K.T.; Immenhauser, A. Marine bivalve shell geochemistry and ultrastucture from modern low pH environments: Environmental effect versus experimental bias. *Biogeosciences* **2012**, *9*, 1897–1914. [CrossRef]
28. Crémière, A.; Lepland, A.; Chand, S.; Sahy, D.; Condon, D.J.; Noble, S.R.; Martma, T.; Thornsnes, T.; Sauer, S.; Brunstad, H. Timescales of methane seepage on the Norwegian margin following collapse of the Scandinavian Ice Sheet. *Nat. Commun.* **2016**. [CrossRef] [PubMed]

29. Haas, A.; Peckmann, J.; Elvert, M.; Sahling, H.; Bohrmann, G. Patterns of carbonate authigenesis at the Kouilou pockmarks on the Congo deep-sea fan. *Mar. Geol.* **2010**, *268*, 129–136. [CrossRef]
30. Stolper, D.A.; Martini, A.M.; Clog, M.; Douglas, P.M.; Shusta, S.S.; Valentine, D.L.; Sessions, A.L.; Eiler, J.M. Distinguishing and understanding thermogenic and biogenic sources of methane using multiply substituted isotopologies. *Geochim. et Cosmochim. Acta* **2015**, *161*, 219–247. [CrossRef]
31. Miyajima, Y.; Watanabe, Y.; Goto, A.S.; Jenkins, R.G.; Sakai, S.; Matsumoto, R.; Hasegawa, T. Archael lipid biomarker as a tool to constrain the origin of methane at ancient methane seeps: Insight into subsurface fluid flow in the geological past. *J. Asian Earth Sci.* **2020**, *189*, 104134. [CrossRef]
32. Himmler, T.; Birgel, D.; Bayan, G.; Pape, T.; Ge, L.; Bohrmann, G.; Peckmann, J. Formation of seep carbonates along the Makran convergent margin, northern Arabian Sea and a molecular and isotopic approach to constrain the carbon isotopic composition of parent methane. *Chem. Geol.* **2015**, *415*, 102–117. [CrossRef]
33. Niemann, H.; Elvert, M.; Hovland, M.; Orcutt, B.; Judd, A.; Suck, I.; Gutt, J.; Joye, S.; Damm, E.; Finster, K.; et al. Methane emission and consumption at a North Sea gas seep (Tommeliten area). *Biogeosciences* **2005**, *2*, 335–351. [CrossRef]
34. Niemann, H.; Elvert, M. Diagnostic lipid biomarker and stable isotope signatures of microbial communities mediating the anaerobic oxidation of methane with sulphate. *Org. Geochem.* **2008**, *39*, 1668–1677. [CrossRef]
35. Pellenard, P.; Tramoy, R.; Pucéat, E.; Huret, E.; Martinez, M.; Bruneau, L.; Thierry, J. Carbon cycle and seawater palaeotemperature evolution at the Middle-late Jurassic transition, eastern Paris Basin (France). *Mar. Pet. Geol.* **2014**, *53*, 30–43. [CrossRef]
36. Aucour, A.-M.; Sheppard, S.M.F.; Savoye, R. ∂^{13}C of fluvial mollusc shells (Rhône River): A proxy for dissolved inorganic carbon? *Limnol. Oceanogr.* **2003**, *48*, 2186–2193. [CrossRef]
37. Gillikin, D.P.; Lorrain, A.; Bouillon, P.W.; Dehairs, F. Stable carbon isotopic composition of *Mytilus edulis* shells: Relation to metabolism, salinity, $\partial^{13}C_{DIC}$ and phytoplankton. *Org. Geochem.* **2006**, *37*, 1371–1382. [CrossRef]
38. Key, M.M., Jr.; Zágorsek, K.; Patterson, W.P. Paleoenvironmental reconstruction of the Early to Middle Miocene Central Paratethys using stable isotopes from bryozoan skeletons. *Int. J. Earth Sci.* **2012**, *102*, 305–318. [CrossRef]
39. Goodwin, C.; Edwards, H.; Breen, J.; Picton, B. *Rathlin Island—A Survey Report from the Nationally Important Marine Features Project 2009–2011*; Northern Ireland Environmental Agency Research and Development Series No. 11/03; Northern Ireland Environmental Protection Agency: Belfast, UK, 2011.
40. Williams, B.; Halfar, J.; Stenede, R.S.; Wartmann, U.G.; Hetzinger, S.; Adey, W.; Lebednik, P.; Joachimski, M. Twentieth Century ∂^{13}C variability in surface water dissolved inorganic carbon record by coralline algae in the northern North Pacific Ocean and the Bering Sea. *Biogeosciences* **2001**, *8*, 165–174. [CrossRef]
41. Doss, W. Large serpulid worm tube aggregates indicate an abrupt mid-Holocene transition from marine to restricted hyposaline conditions. 19th Annual Keck Research Symposium in Geology Proceedings. *Amherst Mass.* **2006**, 33–37. Available online: https://keckgeology.org/files/pdf/symvol/19th/domincanrep/doss.pdf (accessed on 2 July 2020).
42. Cukrov, N.; Cukrov, M.; Lojen, S. C and N stable isotope variability in soft tissue of invasive species (Annelida, Polychaeta) Ficopomatus enigmaticus. In Proceedings of the International Symposium on Isotopes in Hydrology, Marine Ecosystems, and Climate Change Studies, Monaco, 21 March–1 April 2011.
43. Videtich, P.E. Stable isotope composition of serpulids give insights to calcification processes in marine organisms. *Palaios* **1986**, *1*, 189–193. [CrossRef]
44. Jiang, Z.; Wu, K.; Couples, G.; van Dijke, M.; Sorbie, K.S.; Ma, J. Efficient extraction of pore networks from three-dimensional porous media. *Water Resour. Res.* **2007**, *43*, 2578–2584. [CrossRef]
45. Jiang, Z.; van Dijke, M.I.J.; Wu, K.; Couples, G.D.; Sorbie, K.S.; Ma, J. Stochastic pore network generation from 3D rock images. *Transp. Porous Media* **2012**, *94*, 571–593. [CrossRef]
46. Buckman, J.; Chudi, O.; Lewis, H.; Couples, G.; Huang, T.; Jiang, Z. Synthetic digital rock methods to estimate the impact of quartz cementation on porosity and permeability: Assessment of Miocene turbidite sandstones and prediction of deeper Oligocene sandstones, Niger Delta Basin. *J. Pet. Sci. Eng.* **2020**, *184*, 106538. [CrossRef]
47. Zwicker, J.; Smrzka, D.; Gier, S.; Goedert, J.L.; Peckmann, J. Mineralized conduits are part of the uppermost plumbing system of Oligocene methane-seep deposits, Washington State (USA). *Mar. Pet. Geol.* **2015**, *66*, 616–630. [CrossRef]

48. Providence. Licence P1885. Blocks 125/18, 125/19, 125/23, 125/24, 125/25. Rathlin Basin, Offshore Northern ireland, Relinquishment Report April 2016. 2016. Available online: https://itportal.ogauthority.co.uk/web_files/relinqs/jul2016/P1885.pdf (accessed on 2 July 2020).
49. Fyfe, L.-J.C.; Schofield, N.; Holford, S.; Heafford, A.; Raine, R. Geology and petroleum prospectivity of the Larne and Portpatrick basins, North Channel, offshore SW Scotland and Northern Ireland. *Pet. Geosci.* **2020**, *26*, 272–302. [CrossRef]
50. Noble-James, T.; Judd, A.; Diesing, M.; Clare, D.; Eggett, A.; Silburn, B.; Duncan, G. Monitoring shallow methane-derived authigenic carbonate: Insights from a UK Marine Protected Area. *Aquat. Conserv. Mar. Freshw. Ecosyst.* **2020**, *30*, 959–976. [CrossRef]
51. Naehr, T.H. Authigenic carbonate formation at hydrocarbon seeps in continental margin sediments: A comparative study. *Oceanography* **2007**, *54*, 1268–1291. [CrossRef]